THE ASTROPHYSICAL JOURNAL, 412:294–300, 1993 July 20

IRON AND MOLECULAR OPACITIES AND THE EVOLUTION OF POPULATION I STARS

RICHARD B. STOTHERS AND CHAO-WEN CHIN
Institute for Space Studies, NASA/Goddard Space Flight Center, 2880 Broadway, New York, NY 10025
Received 1992 November 23; accepted 1993 January 26

ABSTRACT

Effects of recent opacity revisions on the evolution of Population I stars are explored over the mass range 1.5–60 $M_\odot$. Opacities are due to Iglesias, Rogers, and Wilson (high temperatures) and to Sharp and to Alexander, Johnson, and Rypma (low temperatures). Opacity parameters considered include the angular momentum coupling scheme for iron, the relative iron abundance, the total metal abundance, and diatomic and triatomic molecular sources. Surprisingly, only the total metal abundance exerts an important control over the evolutionary tracks. Blue loops on the H-R diagram during core helium burning can be very sensitive to opacity, but only insofar as the simple formation or suppression of a blue loop is concerned. The blue loops are most robust for stellar masses around 10 $M_\odot$. We confirm, from a comparison of stellar models with observational data, that the total metal abundance is close to solar and that convective core overshooting is likely to be very slight. The new models predict the existence of an iron convection zone in the envelope and a great widening of the main-sequence band in the H-R diagram at luminosities brighter than 10^5 $L_\odot$.

Subject headings: stars: abundances — stars: evolution — stars: interiors — supergiants

1. INTRODUCTION

Radiative opacities are a fundamental, but still vexingly uncertain, ingredient needed to calculate theoretical models of nondegenerate stars. Inside such stars, four temperature regimes with characteristically different major sources of opacity can be identified: $T < 10^4$ K, metal line, H^-, and molecular absorption; $T = 10^4$–10^5 K, hydrogen and helium absorption; $T = 10^5$–10^8 K intensive metal line absorption; and $T > 10^8$ K, scattering by free electrons. The largest uncertainty in the opacity is reflected in two temperature subregions: $T < 5000$ K, where molecules become significant opacity sources, and $T = 10^5$–10^6 K, where heavy metals (especially iron) are the most important sources.

Recent progress has led from the old Los Alamos generation of hydrogenic opacities (Cox & Stewart 1965, 1970; Huebner et al. 1977) into a new generation of opacities, calculated at Livermore with more sophisticated atomic modeling (Rogers & Iglesias 1992, hereafter RI; Iglesias, Rogers, & Wilson 1992, hereafter IRW). A substantial increase of the opacities has occurred within the subregion $T = 10^5$–10^6 K, owing to, first of all, the inclusion of many more metal lines, especially of iron (RI), and, secondly, a better angular momentum coupling scheme for iron, which increases the number of lines still further (IRW). The new theoretical iron opacities, in particular, have been recently confirmed by laboratory experiments (Da Silva et al. 1992). Improvements in the long-neglected molecular opacities have been made by using more molecular species and denser spectral sampling (Alexander, Johnson, & Rypma 1983; Sharp 1992). This has produced significantly larger opacities for $T < 5000$ K.

Employed in stellar models, local opacity increases of this sort translate generally into lower surface luminosities and lower effective temperatures (Cesarsky 1969; Johnson & Whitaker 1975). For very precise and accurate stellar modeling, however, even modest improvements in the radiative opacities can have important consequences. Simple substitution of the RI opacities in place of the Los Alamos opacities, for example, has significantly reduced the implied interior metallicity and implied amount of convective core overshooting in upper main-sequence stars and supergiants (Stothers & Chin 1991).

The purpose of the present paper is to investigate the consequences for stellar evolution of making the following three additional changes in the opacities: the angular momentum coupling scheme used for iron, the relative abundance of iron among the metals, and the inclusion of diatomic and triatomic molecules. IRW have pointed out the crucial importance of iron for the high-temperature opacities, while the previous lack of certainty about the molecular contribution to the low-temperature opacities has been remedied by Sharp (1992) and Alexander et al. (1983) in their detailed studies including the most important molecules. The stellar models computed here represent Population I stars of intermediate and high mass in the general solar neighborhood.

2. OPACITIES

2.1. *Low-Temperature Opacities*

The traditional major opacity sources that have been included at low temperatures are absorption by easily ionized metals and by the H^- ion, but no molecular sources. This is true, for example, of the standard Cox & Stewart opacities (1965) that we have long employed, although Cox & Stewart (1970) added one molecule, H_2. Most of our present stellar models are based on opacities without molecules included.

Two recent sets of low-temperature opacities, including molecular sources, are exhibited in Figure 1. The Alexander et al. (1983) opacities and the Sharp (1992) opacities employ the Cameron & Pine (1973) and Cameron (1973) solar mixtures of elements, respectively, which are very similar to each other. The Sharp opacities tend to be somewhat larger than the Alexander et al. ones for $\log T > 3.7$, but the converse is true where molecules are important. Nonetheless, differences remain fairly small over most of the temperature range above $\log T = 3.5$, which is of interest in this paper. Moreover, a better treatment of H_2O by Alexander, Augason, & Johnson (1989) has brought the Alexander et al. (1983) opacities closer to Sharp's (1992) values for $\log T < 3.7$.

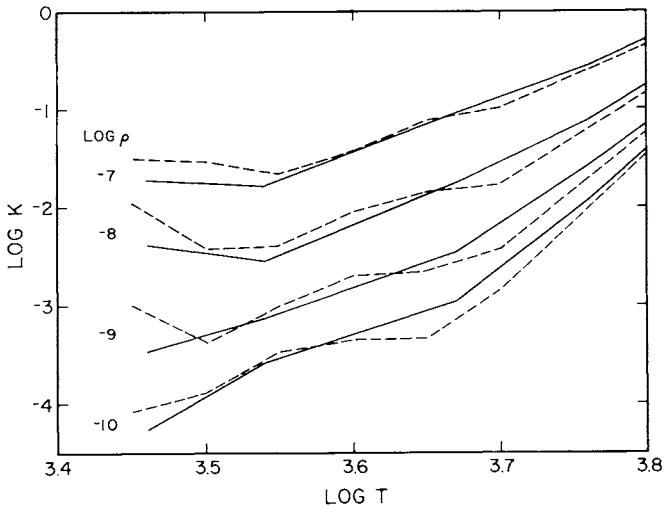

FIG. 1.—Low-temperature opacities due to Alexander et al. (1983) (*dashed lines*) and Sharp (1992) (*solid lines*) as a function of temperature, for four stellar-envelope densities.

Accordingly, a simple formula consisting of straight-line segments has been fitted to the average of the two sets of opacities so as to cover the temperature range $3.45 \leq \log T \leq 3.80$ and the density range $-9 \leq \log \rho \leq -7$, while matching very closely the RI/IRW opacities at $\log T = 3.78$, where the Livermore tables terminate. The fit also extrapolates well down to $\log \rho = -10$ if $\log T \leq 3.50$. We find (in cgs units):

$$\log \kappa = 12.38 + 4.73 \log \rho - (2.48 + 1.12 \log \rho) \log T ,$$

for $3.55 \leq \log T \leq 3.80$, and

$$\log \kappa = 31.95 + 4.30 \log \rho - (8.00 + 1.00 \log \rho) \log T ,$$

for $3.45 \leq \log T \leq 3.55$. The fit of these formulae is continuous at $\log T = 3.55$. Although Alexander et al. (1983) have shown that low-temperature opacities in the above range are not very sensitive to minor variations of chemical composition, the fitted formulae apply, strictly speaking, to the following group element abundances by mass: $X = 0.71$ (hydrogen) and $Z = 0.02$ (metals). These represent solar abundances.

2.2. *High-Temperature Opacities*

The RI atomic opacities assume pure LS coupling for all of the chemical elements. Inasmuch as this is a poor approximation for the heavier elements, IRW replaced LS coupling with intermediate coupling for the only abundant heavy element, iron, by explicitly including the spin-orbit interactions. This increases the opacity by splitting and multiplying the number of iron lines.

The choice of the relative abundances of carbon, nitrogen, and oxygen within the CNO group appears to make little difference for the total opacity (Iglesias & Rogers 1991). This circumstance is fortunate, because the stellar hydrogen-burning reactions process primordial C and O into N, some of which later gets swept into the outer envelope by convection.

The RI and IRW opacity tables, however, do not extend to temperatures above 10^8 K, where electron scattering dominates. For $T > 10^8$ K, we have adopted the modified Cox-Stewart opacities as used in our previous work (Stothers & Chin 1973).

2.3. *Iron Abundance*

Whatever the true abundance of iron with respect to the other metals may be inside Population I stars is certainly not known very well, but the iron abundance is probably the most crucial uncertain abundance factor for stellar opacities. In their original work, RI adopted the Anders & Grevesse (1989, hereafter AG89) solar mixture of metals, which contains a quite high percentage, 3.1%, of iron by number, determined from spectroscopic analysis of the solar photosphere. Afterward, IRW used the unpublished, revised Grevesse (G91) solar mixture of metals with its significantly lower percentage of iron, 2.2%, which is the meteoritic value. Four recent solar photospheric analyses, using revised *f*-values for Fe I and Fe II, now find agreement with the meteoritic value (Holweger, Heise, & Kock 1990; Holweger et al. 1991; Biémont et al. 1991; Hannaford et al. 1992). (The relative abundances of the other elements differ but little between the AG89 and G91 mixtures.)

Apart from the Sun, the photospheric iron abundance has been measured with high accuracy for relatively few stars. Fine spectral analyses of several normal, bright B-type main-sequence stars, where interpretational problems are expected to be minimal, have yielded the iron abundances (derived primarily from Fe III) as listed in Table 1. Values of log (Fe/H), where Fe/H represents the iron-to-hydrogen ratio by number of atoms, range from −4.4 to −4.8, with a mean of −4.6. The moderate spread around the mean could arise from cosmic variations of the total metals content *m*, a true scatter of Fe/*m*, differences of analytical techniques and atomic constants, measurement errors, or a combination of these factors. At any rate, Table 1 suggests that Fe/*m* probably does not vary by more than a factor of 2 for young Population I stars in the solar neighborhood. The Sun's photosphere shows log (Fe/H) = -4.5 ± 0.03 (revised value), which is not significantly different from the mean for nearby B stars. Moreover, the mode of the distribution of Fe/H values for all Population I stars having iron abundance determinations is close to solar (Cayrel de Strobel et al. 1992).

3. NEW EVOLUTIONARY SEQUENCES

Stellar models computed for the present study are based on the following input physics, where the notation used is conventional.

TABLE 1

IRON ABUNDANCES IN NORMAL BRIGHT B-TYPE STARS

Star	Spectral Type	log (Fe/H)	Reference
τ Sco	B0 V	−4.7	Hardorp & Scholz 1970
λ Lep	B0.5 IV	−4.5	Hardorp & Scholz 1970
ι Her	B3 V	−4.4 ± 0.2	Peters & Aller 1970
	...	−4.6	Kodaira & Scholz 1970
HD 58343	B3 Ve	−4.6	Kodaira & Scholz 1970
γ Peg	B2 IV	−4.6 ± 0.1	Peters 1976
23 Cas	B8 III	−4.5 ± 0.3	Allen 1977
ν Cap	B9.5 V	−4.6 ± 0.3	Allen 1977
	...	−4.5 ± 0.1	Lemke 1989
	...	−4.5	Adelman 1991
21 Peg	B9.5 V	−4.8 ± 0.2	Sadakane 1981
NGC 6611−254	B2	−4.7	Brown et al. 1986
HD 1999	B6 III	−4.8 ± 0.2	Keenan et al. 1986
F 29	B3 V	−4.4	Keenan et al. 1986
τ Her	B5 IV	−4.8 ± 0.1	Adelman 1988, 1991
π Cet	B7 V	−4.7 ± 0.1	Adelman 1991
134 Tau	B9 IV	−4.6	Adelman 1991
21 Aql	B8 II–III	−4.8	Adelman 1991

TABLE 2

EVOLUTIONARY SEQUENCES BASED ON TWO DIFFERENT ATOMIC COUPLING SCHEMES FOR IRON

$M/M_\odot$	Coupling Scheme	τ_H (10^6 yr)	τ_{He}/τ_H	τ_b/τ_r	ZAMS		TAMS		Blue Tip	
					log $(L/L_\odot)$	log T_e	log $(L/L_\odot)$	log T_e	log $(L/L_\odot)$	log T_e
1.5	Pure LS	2990.02	...	...	0.567	3.835	0.651	3.749	...	...
	Intermediate	2983.72	...	...	0.567	3.837	0.651	3.755	...	...
2	Pure LS	1264.06	...	...	1.079	3.922	1.199	3.813	...	...
	Intermediate	1264.19	...	...	1.079	3.921	1.199	3.813	...	...
2.5	Pure LS	664.497	...	...	1.470	3.991	1.618	3.884	...	...
	Intermediate	664.729	...	...	1.470	3.990	1.618	3.882	...	...
3	Pure LS	399.813	0.232	0.000	1.786	4.046	1.962	3.944	...	...
	Intermediate	401.819	0.236	0.000	1.786	4.045	1.962	3.941	...	...
5	Pure LS	100.047	0.175	0.000	2.638	4.196	2.882	4.110	...	...
	Intermediate	100.179	0.169	0.000	2.638	4.195	2.881	4.108	...	...
7	Pure LS	45.044	0.158	0.583	3.169	4.288	3.446	4.209	3.584	3.943
	Intermediate	44.984	0.164	0.474	3.169	4.286	3.443	4.208	3.570	3.926
10	Pure LS	21.880	0.130	1.118	3.696	4.377	3.993	4.298	4.154	4.096
	Intermediate	21.920	0.133	0.973	3.695	4.375	3.990	4.295	4.141	4.088
15	Pure LS	11.522	0.104	0.578	4.254	4.466	4.567	4.372	4.726	4.203
	Intermediate	11.535	0.103	0.568	4.250	4.464	4.564	4.367	4.722	4.191
30	Pure LS	5.498	...	...	5.055	4.584	5.324	4.429	...	...
	Intermediate	5.513	...	...	5.054	4.581	5.321	4.395	...	...
60	Pure LS	3.475	...	...	5.701	4.666	5.881	4.406	...	...
	Intermediate	3.527	...	...	5.697	4.652	5.861	4.151	...	...

NOTE.—$Z_e = 0.03$ and the AG89 solar mixture were used.

TABLE 3

EVOLUTIONARY SEQUENCES AT INTERMEDIATE TO HIGH MASSES FOR VARIOUS CHEMICAL MIXTURES

Z_e	Metals Mixture	ZAMS		TAMS		Red Top		Red Bottom		Blue Tip	
		log $(L/L_\odot)$	log T_e	log $(L/L_\odot)$	log T_e	log $(L/L_\odot)$	log T_e	log $(L/L_\odot)$	log T_e	log $(L/L_\odot)$	log T_e
					3 $M_\odot$						
0.02	AG89	1.877	4.081	2.074	3.983	2.217	3.634	1.937	3.666	...	...
0.02	G91	1.895	4.086	2.079	3.993	2.181	3.635	1.925	3.666	...	...
0.02	G91 + Mol.	1.895	4.086	2.079	3.993	2.170	3.603	1.898	3.631	...	...
0.03	AG89	1.786	4.045	1.962	3.941	2.133	3.623	1.743	3.655	...	...
0.03	G91	1.806	4.051	1.970	3.953	2.097	3.624	1.737	3.652	...	...
					5 $M_\odot$						
0.02	AG89	2.706	4.225	2.949	4.144	3.016	3.621	2.916	3.636	...	...
0.02	G91	2.723	4.229	2.958	4.149	3.052	3.618	2.864	3.642	...	...
0.02	G91 + Mol.	2.723	4.229	2.958	4.149	3.046	3.581	2.831	3.606	...	...
0.03	AG89	2.638	4.195	2.881	4.108	3.002	3.607	2.743	3.639	...	...
0.03	G91	2.657	4.201	2.883	4.117	2.961	3.610	2.772	3.633	...	...
					7 $M_\odot$						
0.02	AG89	3.222	4.312	3.492	4.237	3.563	3.596	3.396	3.620	...	...
0.02	G91	3.237	4.316	3.500	4.241	3.585	3.593	3.367	3.624	3.598	3.844
0.02	G91 + Mol.	3.237	4.316	3.500	4.241	3.581	3.557	3.328	3.588	3.677	3.977
0.03	AG89	3.169	4.286	3.433	4.208	3.533	3.584	3.236	3.624	3.570	3.926
0.03	G91	3.186	4.291	3.441	4.212	3.547	3.582	3.235	3.624	3.587	3.953
					10 $M_\odot$						
0.02	AG89	3.735	4.396	4.031	4.320	4.143	3.566	3.908	3.600	4.221	4.121
0.02	G91	3.748	4.400	4.040	4.324	4.149	3.565	3.918	3.600	4.229	4.128
0.02	G91 + Mol.	3.748	4.400	4.040	4.324	4.147	3.529	3.889	3.562	4.221	4.134
0.03	AG89	3.695	4.375	3.990	4.295	4.108	3.553	3.790	3.599	4.141	4.088
0.03	G91	3.710	4.379	3.996	4.300	4.104	3.554	3.802	3.596	4.153	4.095
					15 $M_\odot$						
0.02	AG89	4.278	4.482	4.592	4.390	4.734	3.542	4.525	3.571	...	...
0.02	G91	4.289	4.485	4.597	4.394	4.736	3.541	4.533	3.571	...	...
0.02	G91 + Mol.	4.289	4.485	4.597	4.394	4.735	3.502	4.525	3.532	...	...
0.03	AG89	4.250	4.464	4.564	4.367	4.713	3.528	4.437	3.564	4.722	4.191
0.03	G91	4.263	4.468	4.572	4.371	4.719	3.526	4.450	3.563	4.728	4.200

TABLE 4

STELLAR LIFETIMES AT INTERMEDIATE TO HIGH MASSES FOR VARIOUS CHEMICAL MIXTURES

Z_e	Metals Mixture	τ_H (10^6 yr)	τ_{He}/τ_H	τ_b/τ_r
		3 $M_\odot$		
0.02.....	AG89	329.126	0.231	...
0.02.....	G91	310.440	0.264	...
0.02.....	G91 + Mol.	310.440	0.276	...
0.03.....	AG89	401.819	0.236	...
0.03.....	G91	367.642	0.287	...
		5 $M_\odot$		
0.02.....	AG89	86.530	0.180	...
0.02.....	G91	82.146	0.205	...
0.02.....	G91 + Mol.	82.146	0.205	...
0.03.....	AG89	100.179	0.169	...
0.03.....	G91	93.506	0.200	...
		7 $M_\odot$		
0.02.....	AG89	40.388	0.163	...
0.02.....	G91	39.011	0.164	0.221
0.02.....	G91 + Mol.	39.011	0.173	0.376
0.03.....	AG89	44.984	0.164	0.474
0.03.....	G91	42.787	0.163	0.555
		10 $M_\odot$		
0.02.....	AG89	20.388	0.134	0.697
0.02.....	G91	19.888	0.135	0.702
0.02.....	G91 + Mol.	19.888	0.137	0.705
0.03.....	AG89	21.920	0.133	0.973
0.03.....	G91	21.128	0.139	1.008
		15 $M_\odot$		
0.02.....	AG89	11.014	0.101	...
0.02.....	G91	10.779	0.106	...
0.02.....	G91 + Mol.	10.779	0.104	...
0.03.....	AG89	11.535	0.103	0.568
0.03.....	G91	11.243	0.106	0.462

Initial chemical composition: $X_e = 0.700$ and $Z_e = 0.02$ or 0.03.

Iron abundance: normal, 0.07 Z_e (G91); or high, 0.10 Z_e (AG89).

Low-temperature opacities: atomic plus H^- or atomic plus H^- plus molecular.

High-temperature opacities: Livermore opacities with either LS coupling for iron or intermediate coupling for iron.

Ratio of convective mixing length to local pressure scale height in the outer convection zone: $\alpha_P = 1.4$.

Initial stellar masses: 1.5, 2, 2.5, 3, 5, 7, 10, 15, 30, and 60 $M_\odot$.

Stellar wind mass loss has been ignored, except for initial stellar masses above 15 $M_\odot$ where the parameterized mass-loss rate of Nieuwenhuijzen & de Jager (1990) has been applied. Semiconvection above the hydrogen-burning layers and convective core overshooting have been ignored as being unimportant in these stars (§ 4). The basic prescription as adopted is similar to that used in our original paper using the Livermore opacities, and so enables some useful comparisons to be made.

Evolutionary tracks run, as before, from the zero-age main sequence (ZAMS) to the end of core helium burning in the case of stellar masses of 3, 5, 7, 10, and 15 $M_\odot$. Otherwise, only the main-sequence phase is covered. This phase includes a point of lowest effective temperature (TAMS stage) which occurs not long before central hydrogen is exhausted.

Tables 2–5 summarize the main results. In these tables, τ_H is the core hydrogen-burning lifetime, τ_{He} is the core helium-burning lifetime, and τ_b and τ_r are the fractions of the core helium-burning lifetime that are spent in the blue-supergiant and red-supergiant configurations, respectively. The dividing line between blue and red is taken at log $T_e = 3.70$. The two locations designated as "red top" and "red bottom" refer to the stable stretch of the red giant (or supergiant) branch on the H-R diagram after the star has entered the slow stages of core helium depletion. The "blue tip" refers to the extremum of the subsequent blue loop, if any.

Model results referring to the two atomic coupling schemes for iron are presented in Table 2, where the largest plausible iron abundance was adopted. Although intermediate coupling yields slightly larger opacities than does LS coupling, the effect on the stellar models is virtually nil. Somewhat more noticeable changes that appear at the two highest stellar masses are probably due to the fact that the RI opacity tables had to be extrapolated to very low densities. The extrapolation was done by assuming opacity values at exterior grid points that are equal to the old Cox-Stewart values, which now appear to be too small. Accordingly, the most massive stellar models with opacities ostensibly based on the RI tables with pure LS coupling are somewhat too bright and hot (Stothers & Chin 1991).

All of our other model sequences are based on intermediate coupling for iron, for which the opacity tables (IRW) needed no extrapolation. The astrophysical effects of the iron abundance and the total metal abundance are displayed in Figures 2 and 3, with a summary of the main data being presented in Tables 3 and 4. As is well known, any increase of the opacities due to a greater abundance of atomic absorbers deep in the stellar interior leads to fainter luminosities, cooler effective

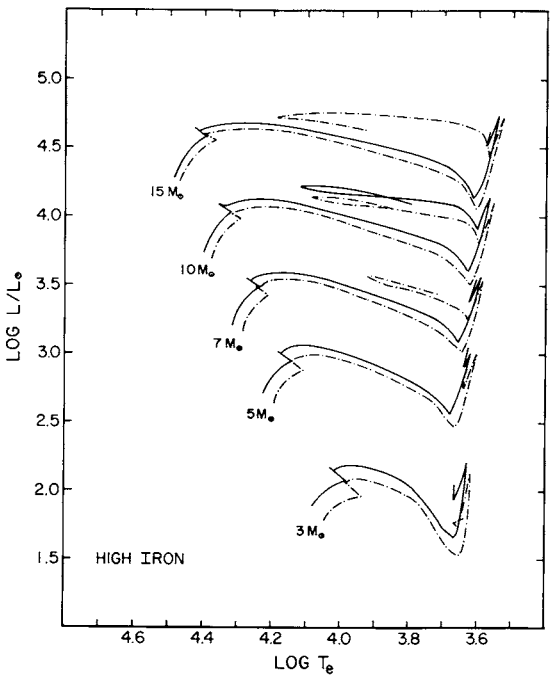

FIG. 2.—Theoretical H-R diagram showing evolutionary tracks running from the ZAMS stage to the end of core helium burning. In the stellar models, Livermore opacities were used with a high-iron (AG89) metals mixture and intermediate coupling for iron. The initial metals abundance was $Z_e = 0.02$ (*solid lines*) or $Z_e = 0.03$ (*dash-dotted lines*).

TABLE 5

MAIN-SEQUENCE EVOLUTION AT LOW AND VERY HIGH MASSES FOR VARIOUS CHEMICAL MIXTURES

Z_e	METALS MIXTURE	τ_H (10^6 yr)	FINAL $M/M_\odot$	ZAMS log $(L/L_\odot)$	ZAMS log T_e	TAMS log $(L/L_\odot)$	TAMS log T_e
			1.5 $M_\odot$				
0.02.....	AG89	2340.27	1.5	0.682	3.874	0.793	3.785
0.02.....	G91	2169.45	1.5	0.703	3.880	0.807	3.792
0.03.....	AG89	2983.72	1.5	0.567	3.837	0.651	3.755
0.03.....	G91	2736.59	1.5	0.591	3.843	0.672	3.762
			2 $M_\odot$				
0.02.....	AG89	1005.07	2.0	1.186	3.961	1.330	3.853
0.02.....	G91	931.70	2.0	1.206	3.966	1.337	3.863
0.03.....	AG89	1264.19	2.0	1.079	3.921	1.199	3.813
0.03.....	G91	1144.07	2.0	1.101	3.928	1.211	3.824
			2.5 $M_\odot$				
0.02.....	AG89	537.249	2.5	1.569	4.027	1.738	3.924
0.02.....	G91	502.946	2.5	1.588	4.033	1.748	3.934
0.03.....	AG89	664.729	2.5	1.470	3.990	1.618	3.882
0.03.....	G91	612.134	2.5	1.492	3.996	1.628	3.894
			30 $M_\odot$				
0.02.....	AG89	5.410	28.21	5.069	4.596	5.338	4.427
0.02.....	G91	5.332	28.23	5.076	4.599	5.340	4.435
0.03.....	AG89	5.513	28.15	5.054	4.581	5.321	4.395
0.03.....	G91	5.433	28.17	5.062	4.584	5.325	4.406
			60 $M_\odot$				
0.02.....	AG89	3.462	48.51	5.707	4.668	5.879	4.253
0.02.....	G91	3.440	48.82	5.711	4.672	5.883	4.270
0.03.....	AG89	3.527	46.84	5.697	4.652	5.861	4.151
0.03.....	G91	3.501	47.09	5.702	4.657	5.869	4.157

temperatures, and longer lifetimes. However, the 40% increase of the iron abundance incurred by changing from the G91 solar mixture to the AG89 solar mixture produces only very small changes in the stellar models if the total metals abundance is held fixed. The single exception occurs in the case where the iron increase suppresses the blue loop at 7 $M_\odot$ for $Z_e = 0.02$. This particular blue loop is very marginal in any case, since its blue tip sits inside, or near, the secularly unstable yellow region of the H-R diagram (Chin & Stothers 1991). Thus it is perhaps not surprising that the comparatively minor addition of *molecular* sources to the total opacity is able, apparently paradoxically, to promote a fully developed blue loop (Tables 3 and 4).

Otherwise, molecular opacities have little effect on any of the tracks, except to shift the red giant (or supergiant) branch to slightly lower effective temperatures. Even this very small temperature shift of 0.04 dex could be in part due to the differences between the low-temperature atomic opacities characterizing the two sets of tracks. In any case, the absolute shift of effective temperature is uncertain, because a concomitant increase of α_P from 1.4 to 1.8 would wipe out the derived relative shift.

By far, the most easily observable effects arise by changing Z_e. A 50% increase of Z_e, for example, triggers a blue loop at 15 $M_\odot$, where one was absent for a solar composition. Yet the extreme sensitivity of the formation of blue loops generally to small changes in input parameters has already been pointed out in detail (Chin & Stothers 1991). As was previously the case for the old Los Alamos opacities, the most robust blue loops occur here for stellar masses around 10 $M_\odot$.

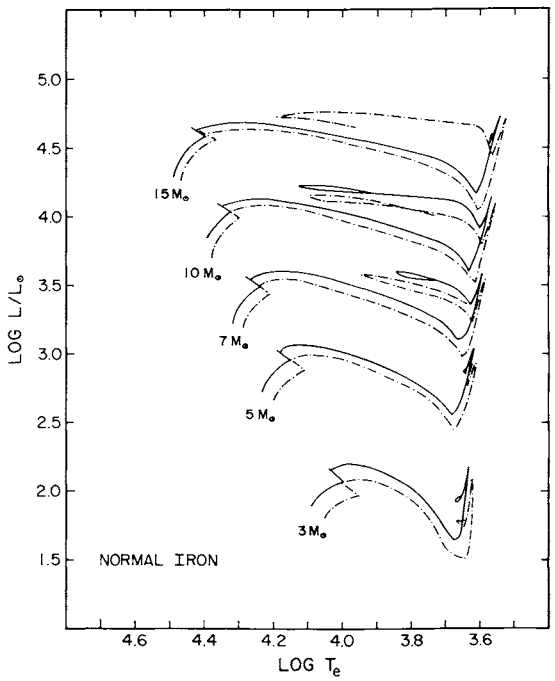

FIG. 3.—Theoretical H-R diagram showing evolutionary tracks running from the ZAMS stage to the end of core helium burning. In the stellar models, Livermore opacities were used with a normal-iron (G91) metals mixture and intermediate coupling for iron. Same notation as for Fig. 2.

An unresolved problem is the theoretically predicted absence of blue loops for masses below 7 $M_\odot$; observationally, blue loops occur down to 4 $M_\odot$. Their predicted absence seems to be independent of Z_e, of the percentage of iron among the metals, and of whether or not molecules are included in the low-temperature opacities. It is possible, however, that future revisions of the opacities, especially opacity increases at temperatures characteristic of the base of the outer convection zone ($\sim 10^6$ K), could lead to blue loops, as this mechanism has worked before (Carson & Stothers 1976). Three other factors that are also known in some cases to trigger blue loops include an increase in the rate of the uncertain $^{12}C(\alpha, \gamma)^{16}O$ reaction, an increase of α_P (or perhaps an equivalent change of convective envelope structure brought about by an improved theory of stellar convection), and a moderate amount of downward convective envelope overshooting (Chin & Stothers 1991). We have verified, however, that physically plausible variations of these three parameters do not lead to blue loops at masses below 7 $M_\odot$ with the present opacities.

Lastly, a summary of results for the main-sequence evolution of stars with both moderately low and very high masses is contained in Table 5. These results confirm what we have already learned by considering the intermediate to high masses.

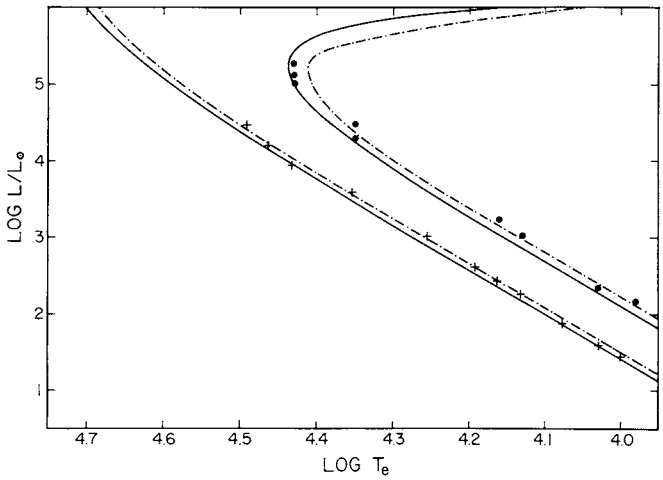

FIG. 4.—H-R diagram for observed O- and B-type stars, showing the standard ZAMS (*plus signs*) and the TAMS based on grouped members of open clusters (*dots*). Theoretical lines for the ZAMS and TAMS refer to $Z_e = 0.02$ (*solid lines*) or $Z_e = 0.03$ (*dash-dotted lines*). In the stellar models, Livermore opacities were used with a normal-iron (G91) metals mixture and intermediate coupling for iron.

4. CONCLUSION

Although the latest revisions of the Livermore opacities and the addition of molecular sources have led to surprisingly minor changes from the preliminary stellar models that we published earlier (Stothers & Chin 1991), it is at least worth presenting an up-to-date comparison of our new stellar models with observations of main-sequence stars in the H-R diagram, using the same observational data as before. Such a critical comparison appears in Figure 4.

Both the ZAMS and the TAMS that we predict agree very closely with the corresponding observed stellar sequences, using a normal metals abundance of $Z_e = 0.02$–0.03. In contrast, the use of the old Los Alamos opacities required $Z_e \approx 0.04$ for even approximately close agreement with observations (Popper 1982; Wolff 1990; Noels et al. 1991; Stothers 1991). Since axial body rotation was not included in our stellar models, the observed stellar sequences could possibly appear a little too cool with respect to the predicted sequences. If so, Figure 4 would imply a preferred value of Z_e closer to solar.

This figure also confirms our previous conclusion about the absence of significant convective core overshooting, because even a moderate amount of overshooting would make the predicted TAMS much cooler than observed. Abundant evidence of various kinds now points to little or no convective core overshooting in upper main-sequence stars (Stothers 1991; Stothers & Chin 1991, 1992; Evans, Arellano Ferro, & Udalska 1992). Schaller et al. (1992), too, find a rather small overshoot distance, which does not exceed the upper limit that we have derived. Why then do Alongi et al. (1991) and Lattanzio et al. (1991) still find substantial convective core overshooting? The reason seems to be that these authors have relied primarily on the use of one star cluster, NGC 1866 in the Large Magellanic Cloud, and on the use of one test, a comparison of red-giant and main-sequence luminosity functions. The main-sequence luminosity function, however, is probably not accurately known for such a crowded and contaminated star field as that observed in NGC 1866. With different observations of the same cluster, Brocato et al. (1989) have found no demonstrable evidence for convective core overshooting. Alongi et al. (1993) now concede that the case is still open for NGC 1866 until the problem of the luminosity functions is resolved. As it happens, the same kind of comparative test using luminosity functions has been independently applied to well-observed young star clusters in the Galaxy (Stothers 1991), and has yielded an upper limit for the overshoot distance that is smaller than the large overshoot distance advocated by Alongi et al. (1991, 1993). Nevertheless, further work along these lines is obviously called for.

Finally, we point out, on the H-R diagram, the enormous flaring of the theoretical main-sequence band above $\sim 30\ M_\odot$, which is reminiscent of a result obtained previously with the old Carson opacities (Stothers & Chin 1977, 1978; Bertelli et al. 1984). Although those opacities are now known to be incorrect, the reasons for the main-sequence widening are the same: a large metals contribution to the total opacity at temperatures of 10^5–10^6 K, in combination with heavy stellar wind mass loss. Just as in the case of those opacities, the large Livermore opacities lead to an additional subphotospheric convection zone (here, an iron convection zone). Although this zone is quite shallow on the ZAMS, it deepens as the star expands, and eventually merges with the hydrogen and helium convection zones when the star becomes a red supergiant.

We thank Forrest J. Rogers, Carlos A. Iglesias, and Brian G. Wilson for generously providing us with their new high-temperature opacity tables. Partial funding support for our work came from DWR, Inc.

REFERENCES

Adelman, S. J. 1988, MNRAS, 230, 671
———. 1991, MNRAS, 252, 116
Alexander, D. R., Augason, G. C., & Johnson, H. R. 1989, ApJ, 345, 1014
Alexander, D. R., Johnson, H. R., & Rypma, R. L. 1983, ApJ, 272, 773
Allen, M. S. 1977, ApJ, 213, 121
Alongi, M., Bertelli, G., Bressan, A., & Chiosi, C. 1991, A&A, 244, 95

Alongi, M., Bertelli, G., Bressan, A., Chiosi, C., Fagotto, F., Greggio, L., & Nasi, E. 1993, preprint
Anders, E., & Grevesse, N. 1989, Geochim. Cosmochim. Acta, 53, 197 (AG89)
Bertelli, G., Bressan, A. G., & Chiosi, C. 1984, A&A, 130, 279
Biémont, E., Baudoux, M., Kurucz, R. L., Ansbacher, W., & Pinnington, E. H. 1991, A&A, 249, 539
Brocato, E., Buonanno, R., Castellani, V., & Walker, A. R. 1989, ApJS, 71, 25
Brown, P. J. F., Dufton, P. L., Lennon, D. J., Keenan, F. P., & Kilkenny, D. 1986, A&A, 155, 113
Cameron, A. G. W. 1973, Space Sci. Rev., 15, 121
Cameron, A. G. W., & Pine, M. R. 1973, Icarus, 18, 377
Carson, T. R., & Stothers, R. B. 1976, ApJ, 204, 461
Cayrel de Strobel, G., et al. 1992, A&AS, 95, 273
Cesarsky, C. J. 1969, ApJ, 156, 385
Chin, C.-w., & Stothers, R. B. 1991, ApJS, 77, 299
Cox, A. N., & Stewart, J. N. 1965, ApJS, 11, 22
———. 1970, ApJS, 19, 243
Da Silva, L. B., et al. 1992, Phys. Rev. Lett., 69, 438
Evans, N. R., Arellano Ferro, A., & Udalska, J. 1992, AJ, 103, 1638
Hannaford, P., Lowe, R. M., Grevesse, N., & Noels, A. 1992, A&A, 259, 301
Hardorp, J., & Scholz, M. 1970, ApJS, 19, 193
Holweger, H., Bard, A., Kock, A., & Kock, M. 1991, A&A, 249, 545
Holweger, H., Heise, C., & Kock, M. 1990, A&A, 232, 510
Huebner, W. F., Merts, A. L., Magee, N. H., & Argo, M. F. 1977, Los Alamos Sci. Rep. LA-6760-M
Iglesias, C. A., & Rogers, F. J. 1991, ApJ, 371, 408
Iglesias, C. A., Rogers, F. J., & Wilson, B. G. 1992, ApJ, 397, 717 (IRW)
Johnson, H. R., & Whitaker, R. W. 1975, MNRAS, 173, 523
Keenan, F. P., Brown, P. J. F., & Lennon, D. J. 1986, A&A, 155, 333
Kodaira, K., & Scholz, M. 1970, A&A, 6, 93
Lattanzio, J. C., Vallenari, A., Bertelli, G., & Chiosi, C. 1991, A&A, 250, 340
Lemke, M. 1989, A&A, 225, 125
Nieuwenhuijzen, H., & de Jager, C. 1990, A&A, 231, 134
Noels, A., Grevesse, N., Magain, P., Neuforge, C., Baglin, A., & Lebreton, Y. 1991, A&A, 247, 91
Peters, G. J. 1976, ApJS, 30, 551
Peters, G. J., & Aller, L. H. 1970, ApJ, 159, 525
Popper, D. M. 1982, ApJ, 254, 203
Rogers, F. J., & Iglesias, C. A. 1992, ApJS, 79, 507 (RI)
Sadakane, K. 1981, PASP, 93, 587
Schaller, G., Schaerer, D., Meynet, G., & Maeder, A. 1992, A&AS, 96, 269
Sharp, C. M. 1992, A&AS, 94, 1
Stothers, R. B. 1991, ApJ, 383, 820
Stothers, R. B., & Chin, C.-w. 1973, ApJ, 179, 555
———. 1977, ApJ, 211, 189
———. 1978, ApJ, 226, 231
———. 1991, ApJ, 381, L67
———. 1992, ApJ, 390, 136
Wolff, S. C. 1990, AJ, 100, 1994